Reprinted from Nature, Vol. 344, No. 6267, pp. 627–632, 12th April, 1990


# Evidence from gravity data for focused magmatic accretion along the Mid-Atlantic Ridge

**J. Lin*, G. M. Purdy*, H. Schouten*, J.-C. Sempere† & C. Zervas†**

* Department of Geology and Geophysics, Woods Hole Oceanographic Institution, Woods Hole, Massachusetts 02543, USA
† School of Oceanography, University of Washington, Seattle, Washington 98195, USA

Gravity data from the Mid-Atlantic Ridge between latitudes 27°50′ N and 30°40′ N show that the accretion of magma at the ridge is focused at discrete centres along the spreading axis. Large positive gravity anomalies equivalent to reductions of almost 50% in crustal thickness are observed over non-transform discontinuities bounding spreading segments.

MID-OCEAN ridges are the diverging spreading boundaries between lithospheric plates at which new oceanic lithosphere is created. Information on the density structure of the ridge axis provides critical constraints on models of magmatic accretion and mantle dynamic processes at diverging plate boundaries. This information is particularly valuable at slow-spreading ridges, such as the Mid-Atlantic Ridge (MAR), where dramatic changes in sea-floor magmatic and tectonic processes have been observed along the ridge axis.

From December 1988 to January 1989, we carried out an extensive SeaBeam bathymetry, gravity and magnetic survey of a 300-km-long section of the MAR, including the Atlantis transform, between latitudes 27°50′ N and 30°40′ N (Fig. 1). This experiment was the second part of a two-leg investigation of the volcanic and magmatic accretion processes along the MAR between the Kane (23°45′ N) and Atlantis (30°05′ N) transforms. The tectonic setting of the MAR in this area has been established from high-resolution bathymetry[1]. This portion of the MAR is spreading at relatively slow rates of 1.2–1.4 cm $yr^{-1}$ (half rate)[2]. Our survey covers six spreading segments which are offset by the 68-km-long Atlantis transform near latitude 30°05′ N and by prominent non-transform discontinuities near latitudes 28°15′, 28°42′, 28°51′ and 29°23′ N (Fig. 2*a*). The morphology of the Atlantis transform is characterized by a narrow strike-slip zone within a deep transform valley that abuts against the ridge segments. In contrast, the offsetting ridge segments at the non-transform discontinuities are not connected by a narrow strike-slip fault zone but by oblique fault-bounded extensional basins. These non-transform discontinuities are associated with off-axis traces of fossil basins (Fig. 2*a*), indicating their persistence with time. Gravity values were recorded along ship tracks using a high-precision BGM3 gravimeter[3] on board the research vessel *Robert D. Conrad*.

Results of this gravity analysis reveal that magmatic accretion on the MAR is highly focused at discrete centres along the ridge axis. Large gravity anomalies, equivalent to variations in crustal thickness of more than 3 km, are observed over spreading segments. Non-transform discontinuities, in addition to the Atlantis transform, are found to be associated consistently with discontinuities in sub-seafloor density structure. This provides clear evidence that minor non-transform discontinuities along the MAR rift valley do not just represent surficial, *en echelon* cracks in the crust responding to external stresses, but are fundamental divisions of the magmatic, crustal-generation processes.

## Anomalous features of gravity field

The free-air gravity anomaly is dominated by the attraction of sea-floor topography. Anomaly lows are associated with the greater depths of the rift valley and the 100°-striking Atlantis fracture-zone valley near latitude 30°05′ N (Fig. 2*b*). The lowest anomalies (less than −90 mgal) appear over the nodal basins at the eastern and western ridge-transform intersections. Discontinuities in the gravity low along the north–south-trending MAR median valley are clearly visible at latitudes 28°15′, 28°42′, 28°51′ and 29°23′ N. All are associated with morphological discontinuities in the median valley. Analyses of magnetic data suggest that a 14-km westward jump of the spreading axis between the Atlantis transform and latitude 29°45′ N occurred about 0.4 Myr ago[4]. The free-air gravity, however, reveals no such discontinuity at latitude 29°45′ N. Dominant positive anomalies appear over topographic highs to the north and south of the Atlantis transform and over the flanks of median valleys. The largest positive anomalies (more than 90 mgal) appear over the highest mountains at the eastern and western 'inside corners', which are bordered by the MAR axis and the active transform.

We subtract from the free-air anomalies the predictable components of the gravity field to produce a map of complete mantle Bouguer anomaly which can be related directly to the sub-seafloor density structure. These components include the attraction of sea-floor topography (water–crust interface), which can be estimated accurately from the three-dimensional SeaBeam bathymetry, and the attraction of relief on the crust–mantle interface, assuming constant crustal thickness and density. Negligible sediment cover (<10 m) exists in the survey area, so its contribution to the gravity field can be ignored. These calculations were carried out using the method described by Kuo and Forsyth[5].

The complete mantle Bouguer anomaly map thus reflects the gravity field arising from density anomalies in the crust or mantle. The most striking feature in this map is the pattern of circular gravity lows centred on all six spreading segments (Fig. 2*c*), which resemble the 'bulls eye'-shaped gravity lows identified[5] in the southern MAR at latitude 32°30′ S. The most prominent of such gravity lows is associated with the morphologically well defined spreading segment immediately south of the Atlantis transform (segment 2). The centre of this low (−30 mgal) is located near the mid-point of the spreading segment. The least pronounced gravity low is associated with a short segment at latitude 28°45′ N (segment 4).

Individual profiles across the strike of the spreading segments clearly reveal a strong increase in mantle Bouguer anomaly away from the spreading axis (Fig. 3). The rate of increase is comparable to the expected effects of density increase in an ageing and cooling lithosphere. A three-dimensional lithospheric thermal model[6] was used to calculate reference gravity fields (Fig. 3). This model assumes a mantle flow field that is induced solely

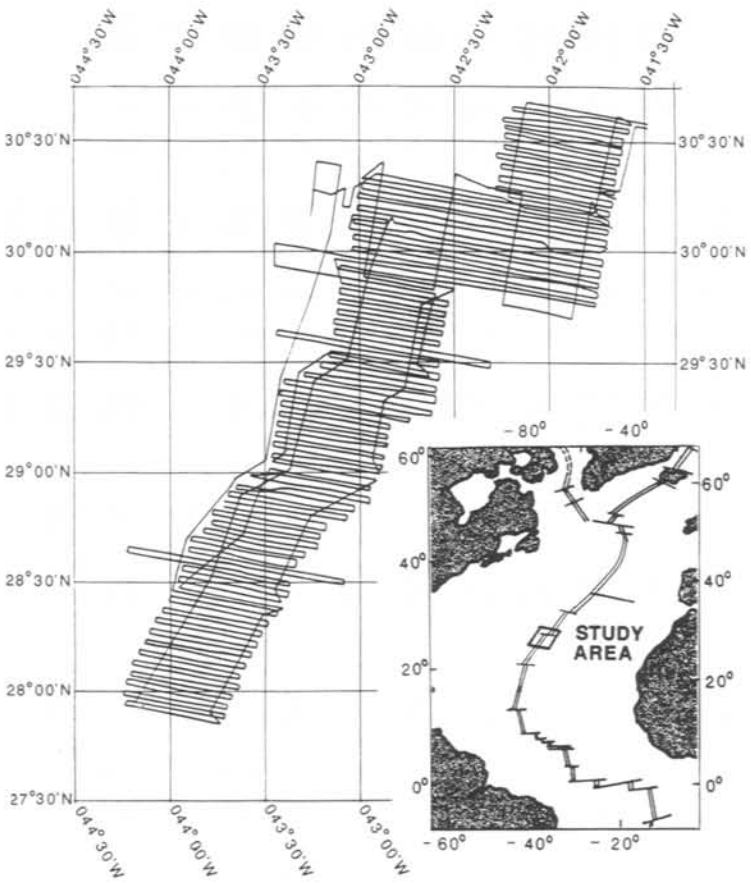


FIG. 1 Location map of survey area. Ship's track denoted by solid lines, along which SeaBeam bathymetry, gravity, and magnetic data were collected. The single and double lines on the index map (inset) represent major fracture zones and spreading centres, respectively.

by the divergence of two surface plates, separating at a constant half speed of 1.4 cm $yr^{-1}$ and passing by each other at the Atlantis transform and the four discontinuities of small offset. A primary feature of the flow induced by plate separation is the relatively uniform mantle upwelling beneath spreading segments, except near large plate-boundary offsets[5,6]. As a result, the calculated structure of the thermal boundary layer (lithosphere) is similar to that of a two-dimensional model except at the Atlantis transform.

The most surprising results of these calculations are the dramatic changes in the observed mantle Bouguer anomaly along the ridge axis, which are not predicted by the thermal model of relatively uniform upwelling. The along-axis profile in Fig. 4*a* illustrates the striking difference between the observed and predicted gravity anomalies. The observed mantle Bouguer anomalies are consistently low at the mid-points of spreading segments and are lowest at segments 2 and 3; the intervening anomaly highs are alway associated with the ends of segments. The anomaly is most positive at the Atlantis transform. In contrast, the thermal model of relatively uniform upwelling predicts significant increases in gravity only near the Atlantis transform at a rate half of the observed value. Near the discontinuities of small offset, the gravity variations predicted by the model of ref. 6 are insignificant. A map of residual anomaly is shown in Fig. 2*d*, and reflects the difference between the mantle Bouguer anomalies (Fig. 2*c*) and the gravity field based on the model of ref. 6.

The remarkable diversity in morphology and gravity anomalies observed along the ridge axis appears to be related to segment length. In our survey area between latitudes 27°50′ N and 30°40′ N, segment 2 is longest (75 km) and is associated with the lowest 'bulls eye'-shaped gravity anomaly (Fig. 2*c*). This is in sharp contrast to the weak gravity low associated with segment 4, which is only 18 km long. Lower values of mantle Bouguer anomalies are observed more frequently at longer spreading segments (Fig. 5*a*).

The relief of the axial depth in the median valley also shows a correlation with segment length. High-resolution SeaBeam

FIG. 2 *a*, SeaBeam bathymetry map contoured at 200-m intervals. The original SeaBeam bathymetric data have been interpolated onto a 1-km grid and machine-contoured. SeaBeam bathymetry data south of latitude 27°50′ N were collected in a previous survey[1]. *b*, Free-air gravity anomaly map contoured at 10-mgal intervals. 3,200-m bathymetric contours are shown to outline the position of the Atlantis fracture zone and rift valleys. Standard Eötvös corrections were made to the raw gravity data[3]. The root-mean-square misfit of the data at 270 survey line crossing points is 1.8 mgal, with a standard deviation of 2.9 mgal. The map was constructed by interpolating the data along ship tracks onto a grid spaced at 1 km and by filling the gaps with data extrapolated according to a minimum-curvature criterion. *c*, Mantle Bouguer anomaly map contoured at 5-mgal intervals. Zero level is arbitrary. Mantle Bouguer anomalies were generated by subtracting from the free-air anomaly the attraction of sea-floor topography and the attraction of relief on the crust–mantle interface. The two-dimensional fast Fourier transform (FFT) approach of Parker[26] was used for calculating gravity fields due to density interfaces. The nominal crust was assumed to be 6 km thick. Densities of 1.03, 2.7, and $3.3\times10^{6}$ g $m^{-3}$ were assumed for sea water, crust and mantle respectively. Maps of density interfaces were interpolated and extrapolated into a rectangular array of 1-km spacing grids and mirrored on edges of the map to reduce edge effects to less than 2 mgal within 3 km. The locations of representative profiles shown in Fig. 3 are marked by dashed lines. *d*, Residual anomaly map contoured at 5-mgal intervals. Zero level is arbitrary. Notice that high anomalies exist near the Atlantis fracture zone and non-transform discontinuities at latitudes 28°15′, 28°42′, 28°51′ and 29°23′ N. This residual anomaly map is calculated by subtracting from the observed mantle Bouguer anomaly the gravity due to lithospheric cooling, based on the model of ref. 6.

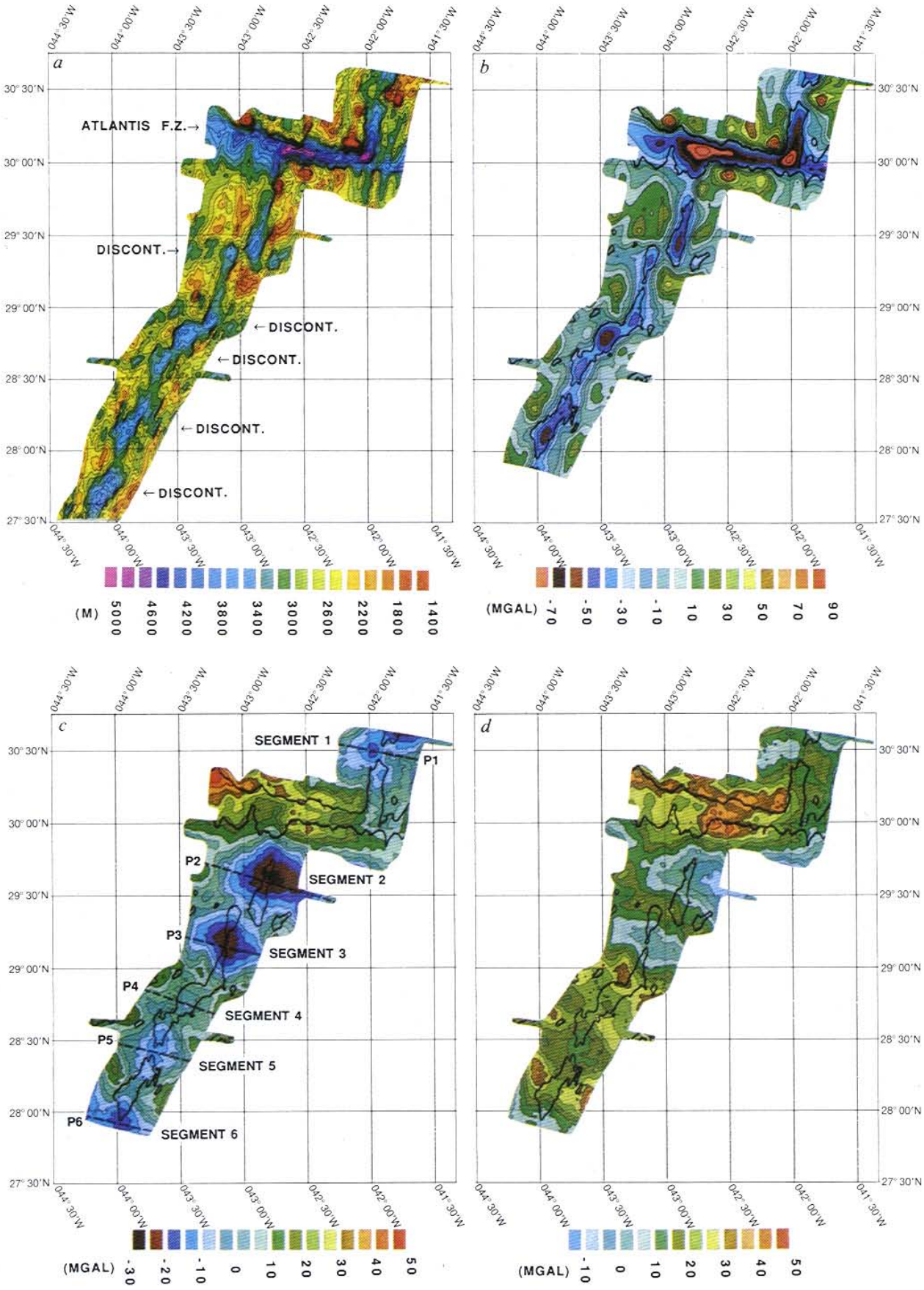
a
ATLANTIS F.Z.→
DISCONT.→
←DISCONT.
←DISCONT.
←DISCONT.
←DISCONT.
(M) 5000 4600 4200 3800 3400 3000 2600 2200 1800 1400
b
(MGAL) -70 -50 -30 -10 10 30 50 70 90
c
SEGMENT 1
SEGMENT 2
SEGMENT 3
SEGMENT 4
SEGMENT 5
SEGMENT 6
P1
P2
P3
P4
P5
P6
(MGAL) -30 -20 -10 0 10 20 30 40 50
d
(MGAL) -10 0 10 20 30 40 50
044° 30'W
044° 00'W
043° 30'W
043° 00'W
042° 30'W
042° 00'W
041° 30'W
30° 30'N
30° 00'N
29° 30'N
29° 00'N
28° 30'N
28° 00'N
27° 30'N

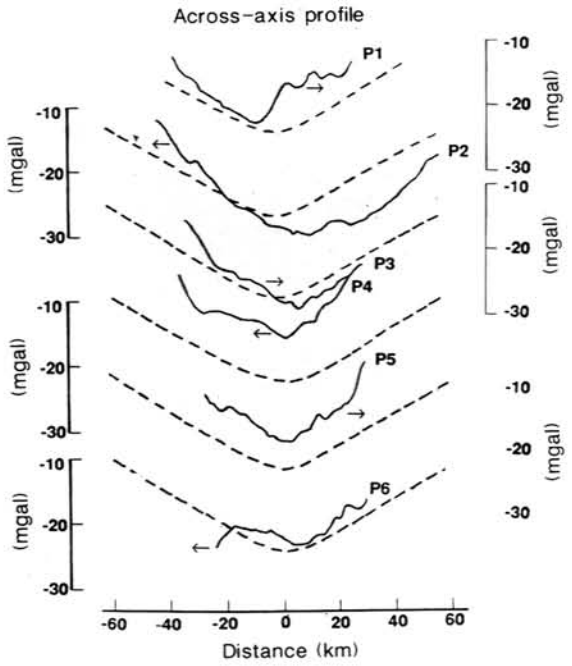


FIG. 3 A comparison between the observed anomalies (solid lines) and the predicted gravity resulting from lithospheric cooling for model of ref. 6 (dashed lines) at representative profiles across six spreading segments. Profile locations are shown in Fig. 2*c*. This three-dimensional thermal model assumes temperatures of 0 °C at the sea floor and 1,350 °C at a depth of 100 km. Temperatures were converted to density changes by multiplying by a thermal expansion coefficient of $3.4 \times 10^{5}$ °C$^{-1}$, a value close to that estimated from sea-floor subsidence with age[5,27]. We then calculate the gravity signals at sea level that result from these density changes.

bathymetric mapping of the MAR between the Kane transform (23°45′ N) and the Atlantis transform (30°05′ N) reveals that there are no other transforms in this 800-km portion of the spreading centre; this plate boundary is composed of 15 segments of varying length separated only by non-transform discontinuities[1]. A compilation of data points for these 15 spreading segments clearly reveals that longer segments have greater topographic relief (Fig. 5*b*). This correlation has also been found for spreading segments at other portions of the MAR and at other ridges[7].

## Models of sub-seafloor density structure

We postulate that the collective effects of significant along-axis changes in the crustal thickness and the density of shallow mantle are the primary sources of the strong mantle Bouguer anomalies along the MAR axis. We examine two limiting models in which the sole source of the residual gravity anomalies is assumed to be either changes in crustal thickness or variations in mantle density. Although the gravity data alone are insufficient to distinguish the direct contribution from each of these sources, the analysis of the data does yield valuable constraints on acceptable values in each model. The density structure constrained by the gravity data is consistent with a physical model in which both the melting of mantle rocks and the buoyancy-driven upwelling of mantle flows are highly focused beneath discrete centres along the MAR axis.

**Source A: Along-axis variations in crustal thickness.** The first model considers lateral changes in crustal thickness. To obtain an upper bound on the maximum possible changes in crustal thickness, we assumed that variations in crustal thickness were the sole source of the residual anomalies shown in Fig. 2*d*. The model crustal layer that results is consistently thicker beneath mid-portions of spreading segments and is thinner beneath ridge discontinuities (Fig. 4*b*). In segment 3, for example, the calculated crustal thickness ranges from 7.5 km at its centre to only 4 km at the southern end, nearly a 50% change in thickness. Because it has a greater length of thicker crust, the volume of crust generated over one million years at segment 3 would be eight times that at segment 4.

An important result from this crustal model is that significant crustal thinning occurs not only at the large offset Atlantis transform but also at the non-transform discontinuities of small offset. Magnetic data for the Atlantic basin show persistent disruptions in magnetic stripes at the off-axis traces of axial discontinuities[8,9]. Seismic refraction studies at a few MAR discontinuities of small offset have shown that some are associated with crustal thinning[10-14]. Our crustal model based on the gravity data provides independent evidence that non-transform discontinuities are fundamental boundaries of ridge magmatic segmentation.

**Source B: Along-axis variations in mantle density.** The second model considers lateral variations in the mantle density. We assume that each spreading segment is fed from below by a

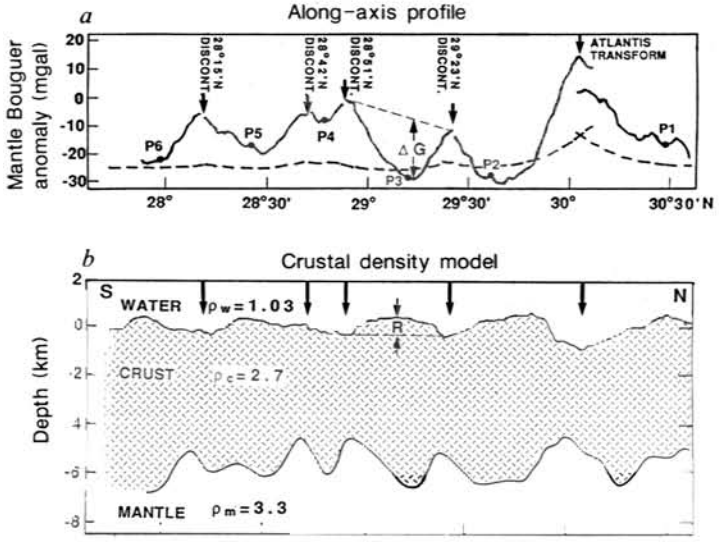


FIG. 4 *a*, Along-axis profile of mantle Bouguer anomaly (solid line) and predicted gravity of the model of ref. 6 (dashed line). Bold numbers denote crossing points with profiles of Fig. 3. $\Delta G$ is the change of mantle Bouguer gravity anomaly within a segment of length *L*. *b*, A cross-sectional view of the crustal structure along the MAR. Along-axis profile of sea-floor depth is shown by the upper boundary of the shaded region. *R* is axial topographic relief within a segment of length *L*. The theoretically calculated relief at the crust–mantle interface is shown by the lower boundary of the shaded region. The model of crustal density assumes that the residual gravity anomalies of Fig. 2*d* are due solely to lateral variations in crustal thickness. The residual gravity signal was continued downwards to the bottom of a 6-km crust and converted into crustal thickness assuming a crust–mantle density contrast of $0.6 \times 10^{6}$ g m$^{-3}$. To prevent amplification of an unrealistic short-wavelength signal in the process of downward continuation, features with wavelength shorter than 25 km were filtered out.

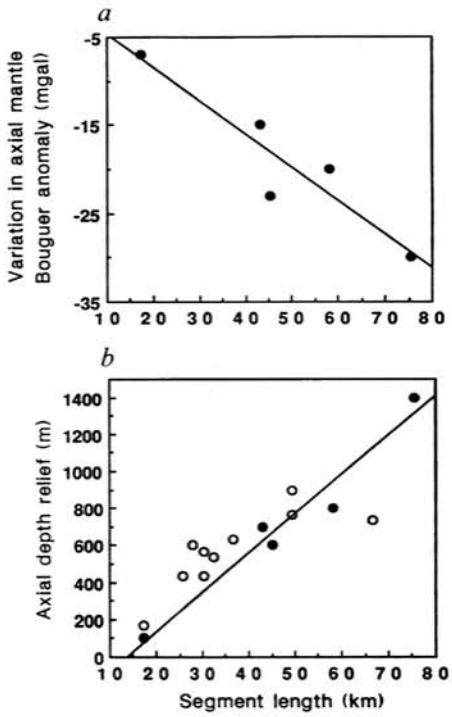


FIG. 5 *a*, Plot of change in mantle Bouguer anomaly within a segment ($\Delta G$) against segment length ($L$) for five segments in this survey area. Notice that longer segments are associated with lower gravity anomalies. *b*, Plot of axial topographic relief ($R$) against segment length $L$ for 15 spreading segments between the Kane and Atlantis transforms. Filled circles correspond to the segments between latitudes 27°50′N and 30°45′N. Open circles correspond to segments between the Kane transform and latitude 27°50′N (ref. 1). Notice that longer segments have greater depth relief.

buoyancy-driven mantle plume which ascends from a zone of partial melt at depth (Fig. 6). This pattern of focused mantle upwelling has two direct effects on the mantle density structure. First, regions of ascending mantle flow are associated with negative density anomalies that result from anomalously high mantle temperatures as described by $\Delta\rho = -\rho_0\alpha\Delta T$, where $\rho_0$ is a reference density, $\alpha$ the coefficient of thermal expansion and $\Delta T$ the excess in mantle temperature. Second, additional negative density anomalies occur in the same regions because of the presence of residual mantle or small amounts of trapped basaltic melts (both are less dense than the unmelted parental mantle[15]). After 20% of melt extraction, for example, the density reduction in the residual mantle is equivalent to the thermal expansion that would be associated with a temperature increase of 500 °C.

If variations in mantle density were the sole source of the residual anomalies in Fig. 2*d*, we estimate that the along-axis mantle density changes would be as large as those associated with the lithospheric cooling across the ridge axis. In segment 3, for example, the required density anomalies are equivalent to a 7-km thickening of the thermal boundary layer from the mid-point of the segment to its distal ends. We also notice that the residual anomalies for segments 2 and 3 are elongated in the direction of plate spreading, whereas that of segment 5 remains 'bulls eye'-shaped (Fig. 2*d*). If the residual anomalies are caused solely by thermally induced variations in mantle density, the mantle upwelling beneath segments 2 and 3 must take the form of two-dimensional convective rolls that strike in the direction of plate spreading. Alternatively, the mantle density anomalies at the ridge axis might be 'frozen' in the ageing lithosphere and be carried away from the ridge axis.

## Implications for mechanisms of magmatic accretion

The density structure of the crust and that of the mantle are related by their common origin in mantle melting and upwelling. Beneath mid-portions of spreading segments, enhanced melting and the excess mantle temperature of the hypothesized ascending plume can cause negative density anomalies in the mantle. The same processes can produce excess amounts of melt which

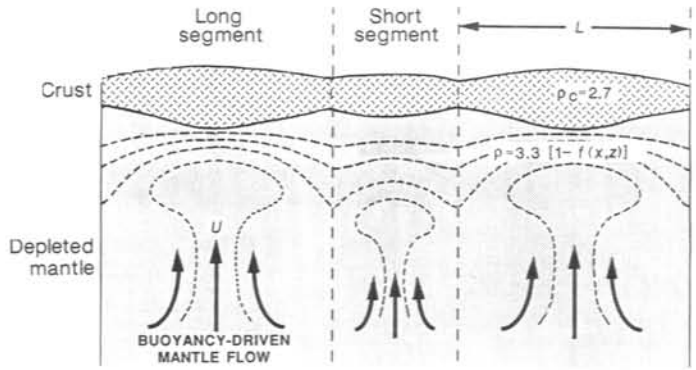


FIG. 6 The preferred model of MAR density structures that are consistent with the results of gravity analyses. We propose that the MAR spreading segments are fed from below by buoyancy-driven mantle flows. Thick solid lines with arrow heads represent mantle flows. Broken curves represent lines of equal density in the mantle. The average crustal density is $2.7\times10^6$ g m$^{-3}$. The mantle density is $\rho = 3.3[1 - f(x,z)]\times10^6$ g m$^{-3}$, where $f(x,z)$ depends primarily on the mantle temperature, the amount of melt extraction and the amount of trapped basaltic melts. $x$ and $z$ are horizontal and vertical coordinates. Over regions of ascending mantle plumes, large temperature gradients and a high degree of decompression melting are expected. This could result in thicker crust and lower mantle densities beneath mid-portions of spreading segments. Both the changes in crustal thickness and variations in mantle density are likely to contribute significantly to the gravity field. A crustal model is shown in Fig. 4*b*, which assumes that the changes of crustal thickness are the sole source of the residual gravity anomalies.

migrate upwards through a porous mantle matrix, or through fractures and veins, to form thicker crust. It is therefore unlikely that significant density anomalies occur only in the crust or only in the mantle. Independent information on the crustal structure, obtainable from seismic studies for example, could be used to constrain the relative importance to the gravity field of each density structure.

It has been proposed that focused mantle upwelling is initiated by a Rayleigh–Taylor gravitational instability developed in the partial melt zone at depth which is overlain by heavier mantle material[16–18]. We argue that, beyond the stage of initiation, it is the strong feedback between the melting and upwelling processes that maintains the stability of each mantle plume. Concentrated melting in regions of ascending mantle plumes can cause a reduction in the mantle viscosity[16,19,20] as well as an increase in the mantle compositional buoyancy[21–23], and both changes favour further focusing of the mantle upwelling into regions of already existing melt. The mantle flow induced by the separation of rigid surface plates, on the other hand, may create horizontal shear stresses in the mantle in the direction of plate spreading. If these stresses are sufficiently large, the originally cylindrical plumes might be deformed into two-dimensional convective rolls oriented in the direction of plate spreading.

The thermal structure of a buoyancy-driven mantle plume depends in part on its geometric dimension: larger mantle plumes ascend faster. To illustrate this in a simple way, we assume that a mantle plume of diameter $L$ is composed of a continuous series of buoyant spherical bodies (Stokes flow) with a density that is less than the surrounding mantle by $\Delta\rho$. The ascent velocity $U$ of a buoyant spherical body is controlled by the balance between the upward buoyancy force, $\Delta\rho g[(4/3)\pi(L/2)^3]$, and the downward viscous drag exerted on the spherical surface, $6\pi\mu(L/2)U$, where $g$ is the acceleration due to gravity and $\mu$ is the viscosity of the surrounding mantle. This gives $U = 2\Delta\rho g(L/2)^2/(9\mu)$, indicating that the ascent velocity is proportional to the square of the plume diameter. For two-dimensional convective rolls, it can also be shown[24] that the ascent velocity of upwelling plumes is proportional to the square of the size of the rolls.

If longer spreading segments are associated with larger buoyancy-driven mantle plumes, we expect higher temperature gradients and a larger degree of decompression melting to occur beneath mid-points of longer spreading segments as the result of faster ascent velocities. This suggests that longer segments are associated with thicker crust and with more-negative mantle density anomalies and therefore more-negative gravity anomalies. This hypothesis is at least qualitatively consistent with the gravity data shown in Fig. 5*a*.

We suggest that both the transform and non-transform discontinuities along the MAR reflect fundamental boundaries between buoyancy-driven mantle plumes. In comparison with minor non-transform discontinuities, large-offset transforms are associated with more profound reduction in magmatic accretion because of the decreased mantle upwelling in the plate-separation-induced flow[6]. This explains the large positive mantle Bouguer anomalies observed over the Atlantis transform (Fig. 4) and the large depth relief of sea floor near large-offset transforms elsewhere at the MAR. Macdonald and others[25] have observed a similar relationship between the major transforms and minor discontinuities along the fast-spreading East Pacific Rise.

We conclude that magmatic accretion along the MAR is a fully three-dimensional process. This three-dimensional variability is characterized by focused magmatic accretion and mantle upwelling at discrete centres along the MAR axis. Non-transform discontinuities as well as transforms are the fundamental boundaries of ridge magmatic segmentation. We propose that the feedback between mantle melting and upwelling is an important mechanism in maintaining the stability of buoyancy-driven mantle plumes. The gravity data collected at the MAR provide critical constraints on models of MAR magmatic accretion and mantle dynamic processes. □

Received 4 December 1989; accepted 15 February 1990.

1. Sempere, J.-C., Purdy, G. M. & Schouten, H. *Nature* (in the press).
2. Klitgord, K. & Schouten, H. in *The Geology of North America* (eds Vogt, P. R. & Tucholke, B. E.) 351–378 (Geological Society of America, Boulder, Colorado, 1986).
3. Bell, R. E. & Watts, A. B. *Geophysics* **51,** 1480–1493 (1986).
4. Zervas, C., Sempere, J.-C., Lin, J. & Purdy, G. M. *Eos* **70,** 1035 (1989).
5. Kuo, B. Y. & Forsyth, D. W. *Mar. geophys. Res.* **10,** 205–232 (1988).
6. Phipps Morgan, J. & Forsyth, D. W. *J. geophys. Res.* **93,** 2955–2966 (1988).
7. Blackman, D. K. & Forsyth, D. W. *Earth planet. Sci. Lett.* **95,** 115–129 (1989).
8. Schouten, H. & White, R. S. *Geology* **8,** 175–179 (1980).
9. Schouten, H. & Klitgord, K. D. *Earth planet. Sci. Lett.* **59,** 255–266 (1982).
10. Mutter, J. C. & Detrick, R. S. *Geology* **12,** 534–537 (1984).
11. White, R. S., Detrick, R. S., Sinha, M. C. & Cormier, M. H. *Geophys. J.R. astr. Soc.* **79,** 779–798 (1984).
12. White, R. S. & Matthews, D. H. *Geophys. J.R. astr. Soc.* **61,** 401–435 (1980).
13. Sinha, M. C. & Louden, K. E. *Geophys. J.R. astr. Soc.* **75,** 713–736 (1983).
14. White, R. S. *et al. Geology* (in the press).
15. Oxburgh, E. R. & Parmentier, E. M. *J. geol. Soc. Lond.* **133,** 343–354 (1977).
16. Whitehead, J. A., Dick, H. B. & Schouten, H. *Nature* **312,** 146–148 (1984).
17. Schouten, H., Klitgord, K. D. & Whitehead, J. A. *Nature* **317,** 225–229 (1985).
18. Crane, K. *Earth planet. Sci. Lett.* **72,** 405–414 (1985).
19. Auer, F., Beckmeimer, H. & Oehlschlegel, G. *J. geophys. Res.* **49,** 89–92 (1981).
20. Buck, W. R. & Su, W. *Geophys. Res. Lett.* **16,** 641–644 (1989).
21. Rabinowicz, M., Ceuleneer, G. & Nicolas, A. *J. geophys. Res.* **92,** 3475–3486 (1987).
22. Scott, D. R. & Stevenson, D. J. *J. geophys. Res.* **94,** 2973–2988 (1989).
23. Sotin, C. & Parmentier, E. M. *Geophys. Res. Lett.* **8,** 835–838 (1989).
24. Turcotte, D. L. & Schubert, G. *Geodynamics* (Wiley, New York, 1983).
25. Macdonald, K. C. *et al. Nature* **335,** 217–225 (1988).
26. Parker, R. L. *Geophys. J.R. astr. Soc.* **31,** 447–455 (1972).
27. Parsons, B. & Sclater, J. G. *J. geophys. Res.* **82,** 803–827 (1977).

ACKNOWLEDGEMENTS. We are indebted to J. Phipps Morgan, B. Y. Kuo and D. Forsyth for allowing us to use their codes of gravity analysis. We thank the officers, crew and scientific personnel of the R/V *Conrad* (leg 2912) for their support at sea. W. Robinson reduced raw gravity data, B. Trams assisted with data collection at sea, and B. Y. Kuo assisted with data analysis. We benefited from discussions with E. M. Parmentier and J. Phipps Morgan and reviews by J. Fox, M. Kleinrock, D. Smith and M. Tivey. This work was funded by the NSF and a WHOI Culpeper Young Scientist Award (J.L.).

Printed in Great Britain by Turnergraphic Limited, Basingstoke, Hampshire